Journal of Sound and Vibration (1997) **201**(4), 407–426

THE EFFECT OF LENGTH ON THE ACOUSTIC ATTENUATION PERFORMANCE OF CONCENTRIC EXPANSION CHAMBERS: AN ANALYTICAL, COMPUTATIONAL AND EXPERIMENTAL INVESTIGATION†

A. Selamet and P. M. Radavich

Department of Mechanical Engineering, *The Ohio State University*, *Columbus*, *OH* 43210, *U.S.A.*

(*Received* 28 *December* 1995, *and in final form* 7 *August* 1996)

Due to their desirable broadband noise attenuation characteristics, expansion chambers are widely used in the ducting systems for pulsating flows, including the breathing systems of engines and reciprocating turbomachinery. The present study investigates in detail the effect of the length on the acoustic attenuation performance of concentric expansion chambers. Three approaches are employed to determine the transmission loss: (1) a two-dimensional, axisymmetric analytical solution; (2) a three-dimensional computational solution based on the boundary element method; and (3) experiments on an extended impedance tube set-up with nine expansion chambers fabricated with fixed inlet and outlet ducts, fixed chamber diameters and varying chamber length to diameter ratios from $l/d = 0{\cdot}2$ to $3{\cdot}5$. The results from all three approaches are shown to agree well. The effect of multi-dimensional propagation is discussed in comparison with the classical treatment for the breakdown of planar waves. The study also provides a simple relation for the number of repeating attenuation domes prior to the domination of higher order modes in terms of the l/d ratio of the expansion chamber.

1. INTRODUCTION

The desirable broad (and repeating) band attenuation of expansion chambers has led to their extensive use as silencers in pulsating flows [1]; including induction and exhaust systems of internal combustion engines, ducts connected to reciprocating pumps and compressors, and fans. For circular concentric chambers, the repeating dome behavior of transmission loss breaks down at a frequency below the onset of the first radial mode. While this breakdown frequency is usually assumed to be dependent only on the radius of the chamber, Craggs [2] showed, using finite element models, that changing the length of the chamber also affected this frequency, with shorter lengths terminating the repeating domes at lower frequencies. El-Sharkawy and Nayfeh [3] later verified Craggs' findings using a three-dimensional analytical solution for concentric chambers. Their analytical results also correlated well with experimental measurements of noise reduction for chambers of different expansion ratios and length to diameter ratios, l/d, ranging from $0{\cdot}3$ to $0{\cdot}9$. Eriksson *et al*. [4] investigated the finite length effects on the transmission loss

† An earlier version of this work was presented at the 1995 SAE International Congress and Exposition, as SAE 950544, in Detroit, Michigan.

0022–460X/97/140407 + 20 $25.00/0/sv960720

of both symmetric (concentric) and asymmetric expansion chambers. This work illustrates that a very short-length concentric expansion chamber no longer exhibits the broadband behavior, and acts rather like a resonator. Ih and Lee [5] developed a three-dimensional analytical model for circular chambers that incorporated mean flow and allowed for offset inlet and outlet locations. Their results matched experimental transmission loss values for l/d ratios ranging from 0·33 to 1·35. They also gave an expression for the l/d ratio where the acoustically short chamber resonance appears. Finally, based on finite element predictions, Sahasrabudhe *et al*. [6] suggested an empirical relation for the approximate number of repeating one-dimensional domes in terms of the l/d ratio of the chamber.

The objective of the present study is to examine in more detail the effect of the circular concentric expansion chamber geometry on the transmission loss characteristics for one-dimensional versus multi-dimensional propagation. Transmission loss results obtained from *two-dimensional acoustical theory* and a *three-dimensional boundary element method* are compared with *experimental results* for nine fabricated expansion chambers with l/d ratios ranging from 0·205 to 3·525. The upper limit represents the outer dimensions of a production vehicle exhaust muffler, and the lower limit ensures a narrow-band peak behavior. The seven configurations in-between are chosen such that each one exhibits a different number (one through seven) of attenuation domes. The boundary element method is also used to predict the pressure field inside the chambers at different frequencies to assess the extent of non-planar propagation prior to the onset of non-planar modes. Finally, an analytical expression is developed and experimentally verified to relate the number of repeating one-dimensional transmission loss domes to the l/d ratio of the chamber.

The study consists of six sections: following this Introduction, section 2 develops and discusses the two-dimensional analytical approach. Sections 3 and 4 provide brief descriptions of the direct boundary element method and the experimental apparatus, respectively. Section 5 compares the results obtained from these three methods, followed by some concluding final remarks in section 6. A brief Appendix is then included on the classical solution of the multi-dimensional wave equation.

2. ANALYTICAL APPROACH

For the concentric configuration of Figure 1 with equal inlet and outlet diameters, d_1, a two-dimensional analytical expression can be obtained for the transmission loss by matching the pressure and velocity at the expansion and the contraction [3, 7, 8]. From

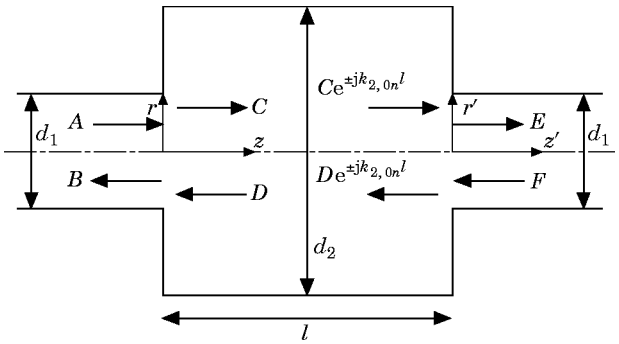

Figure 1. The expansion chamber geometry.

Appendix A, the pressure field for waves travelling in a circular pipe of radius r_i is given as (a list of nomenclature is given in Appendix B)

$$P_A = A_0\, \mathrm{e}^{\mathrm{j}(\omega t - kz)} + \sum_{n=1}^{\infty} A_n \mathrm{J}_0(\gamma_{i,0n} r)\, \mathrm{e}^{\mathrm{j}(\omega t + k_{i,0n} z)} \tag{1}$$

for a wave A travelling in the positive z direction, and

$$P_B = B_0\, \mathrm{e}^{\mathrm{j}(\omega t + kz)} + \sum_{n=1}^{\infty} B_n \mathrm{J}_0(\gamma_{i,0n} r)\, \mathrm{e}^{\mathrm{j}(\omega t - k_{i,0n} z)} \tag{2}$$

for a wave B travelling in the negative z direction, where n designates the radial mode number, A_n the pressure coefficient for each mode, ω the angular frequency, k the planar wave number, J_0 the Bessel function of the first kind of order zero, and $k_{i,0n}$ and $\gamma_{i,0n}$ are the axial and radial wavenumbers given by equations (A3) and (A4). Examining equation (A3) for any radial mode n readily shows that $k_{i,0n}$ will be imaginary when

$$k = \frac{\omega}{c} < \frac{\alpha_{0n}}{r_i} \qquad \text{or} \qquad f < \frac{c}{2\pi}\left(\frac{\alpha_{0n}}{r_i}\right). \tag{3}$$

The sign difference between the planar and radial modes in the exponential terms of equations (1) and (2) ensures that for a wave travelling in the positive direction, the magnitude of all modes, for which equation (3) holds, will decrease exponentially to zero with increasing distance, whereas for negative travelling waves the magnitude must increase. The velocity of waves A and B are obtained from the linearized momentum equation,

$$\rho \frac{\partial U_z}{\partial t} = -\frac{\partial P}{\partial z}, \tag{4}$$

as

$$U_{zA} = \frac{1}{\rho c} A_0\, \mathrm{e}^{\mathrm{j}(\omega t - kz)} - \frac{1}{\rho \omega} \sum_{n=1}^{\infty} A_n k_{i,0n} \mathrm{J}_0(\gamma_{i,0n} r)\, \mathrm{e}^{\mathrm{j}(\omega t + k_{i,0n} z)} \tag{5}$$

and

$$U_{zB} = -\frac{1}{\rho c} B_0\, \mathrm{e}^{\mathrm{j}(\omega t + kz)} + \frac{1}{\rho \omega} \sum_{n=1}^{\infty} B_n k_{i,0n} \mathrm{J}_0(\gamma_{i,0n} r)\, \mathrm{e}^{\mathrm{j}(\omega t - k_{i,0n} z)} \tag{6}$$

At the expansion, the boundary conditions reveal, for the pressure,

$$(P_A + P_B)|_{z=0} = (P_C + P_D)|_{z=0}, \qquad 0 \leqslant r \leqslant r_1 \tag{7}$$

and, for the velocity,

$$(U_{zA} + U_{zB})|_{z=0} = (U_{zC} + U_{zD})|_{z=0}, \qquad 0 \leqslant r \leqslant r_1, \tag{8}$$

$$(U_{zC} + U_{zD})|_{z=0} = 0, \qquad r_1 \leqslant r \leqslant r_2. \tag{9}$$

In these boundary conditions, equations (1) and (5) will be used for waves A, C and E

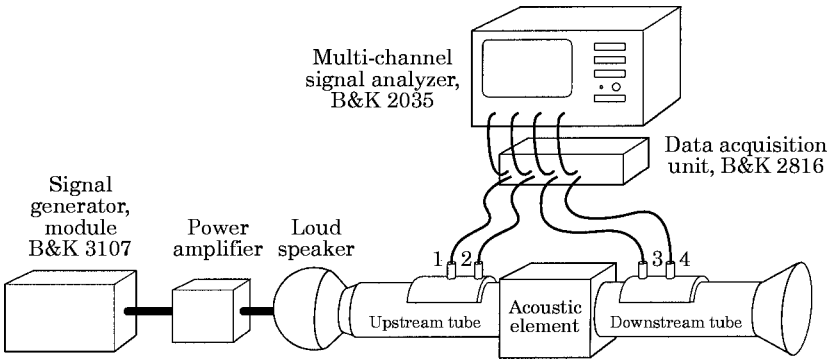

Figure 2. The experimental set-up.

travelling in the positive z direction, and equations (2) and (6) are used for waves B, D and F travelling in the negative direction. For the expansion chamber in Figure 1, the dimensions of the inlet pipe are assumed such that the incoming wave A is planar, and its magnitude, A_0, is chosen to be unity for convenience. An anechoic termination is imposed at the exit of the chamber by setting the reflected wave F to zero.

Following the work of Miles [7], the pressure boundary condition at the expansion can be evaluated by multiplying both sides of equation (7) by $r\,\mathrm{d}r$ for $s = 0$ and integrating from $r = 0$ to $r = r_1$ to give

$$B_0\left(\frac{r_1^2}{2}\right) - C_0\left(\frac{r_1^2}{2}\right) - \sum_{n=1}^{\infty} C_n\left[\frac{r_1 \mathrm{J}_1(\gamma_{2,0n} r_1)}{\gamma_{2,0n}}\right] - D_0\left(\frac{r_1^2}{2}\right) - \sum_{n=1}^{\infty} D_n\left[\frac{r_1 \mathrm{J}_1(\gamma_{2,0n} r_1)}{\gamma_{2,0n}}\right] = -\left(\frac{r_1^2}{2}\right). \tag{10}$$

For $s = 1, 2, , \ldots, \infty$, multiplying both sides of equation (7) by the orthogonal Bessel function term $\mathrm{J}_0(\gamma_{1,0s} r) r\,\mathrm{d}r$ and integrating from $r = 0$ to $r = r_1$ gives

$$B_s\left[\frac{r_1^2}{2}\mathrm{J}_0^2(\gamma_{1,0s} r_1)\right] - \sum_{n=1}^{\infty} C_n\left[\frac{\gamma_{2,0n} r_1 \mathrm{J}_1(\gamma_{2,0n} r_1)\mathrm{J}_0(\gamma_{1,0s} r_1)}{\gamma_{2,0n}^2 - \gamma_{1,0s}^2}\right]$$

$$- \sum_{n=1}^{\infty} D_n\left[\frac{\gamma_{2,0n} r_1 \mathrm{J}_1(\gamma_{2,0n} r_1)\mathrm{J}_0(\gamma_{1,0s} r_1)}{\gamma_{2,0n}^2 - \gamma_{1,0s}^2}\right] = 0 \tag{11}$$

For the two velocity boundary conditions, multiply equations (8) and (9) by $r\,\mathrm{d}r$ and integrate equation (8) from $r = 0$ to $r = r_1$ and equation (9) from $r = r_1$ to $r = r_2$. Adding these two integral equations and simplifying produces, for $s = 0$,

$$-B_0 r_1^2 - C_0 r_2^2 + D_0 r_2^2 = -r_1^2. \tag{12}$$

Similarly, for $s = 1, 2, , \ldots, \infty$, multiplying equations (8) and (9) by $\mathrm{J}_0(\gamma_{2,0s} r) r\,\mathrm{d}r$ and integrating over the same limits yields

TABLE 1

Expansion chamber geometry ($d_1 = 4{\cdot}859$ *cm*, $d_2 = 15{\cdot}318$ *cm*; $m = 9{\cdot}938$)

Geometry	l (cm)	l/d_2
1	3·139	0·205
2	9·371	0·612
3	15·689	1·024
4	21·981	1·435
5	28·230	1·843
6	34·552	2·256
7	40·838	2·666
8	47·113	3·076
9	54·000	3·525

$$-kB_0\left[\frac{r_1 \mathrm{J}_1(\gamma_{2,0s} r_1)}{\gamma_{2,0s}}\right] + \sum_{n=1}^{\infty} B_n k_{1,0n}\left[\frac{\gamma_{2,0s} r_1 \mathrm{J}_1(\gamma_{2,0s} r_1)\mathrm{J}_0(\gamma_{1,0n} r_1)}{\gamma_{2,0s}^2 - \gamma_{1,0n}^2}\right]$$

$$+k_{2,0s}C_s\left[\frac{r_2^2}{2}\mathrm{J}_0^2(\gamma_{2,0s} r_2)\right] - k_{2,0s}D_s\left[\frac{r_2^2}{2}\mathrm{J}_0^2(\gamma_{2,0s} r_2)\right] = -k\left[\frac{r_1 \mathrm{J}_1(\gamma_{2,0s} r_1)}{\gamma_{2,0s}}\right]. \tag{13}$$

The boundary conditions at the contraction require, for the pressure,

$$(P_C + P_D)|_{z=l} = (P_E + P_F)|_{z'=0}, \qquad 0 \leqslant r \leqslant r_1 \tag{14}$$

and, for the velocity,

$$(U_{zC} + U_{zD})|_{z=l} = (U_{zE} + U_{zF})|_{z'=0}, \qquad 0 \leqslant r \leqslant r_1, \tag{15}$$

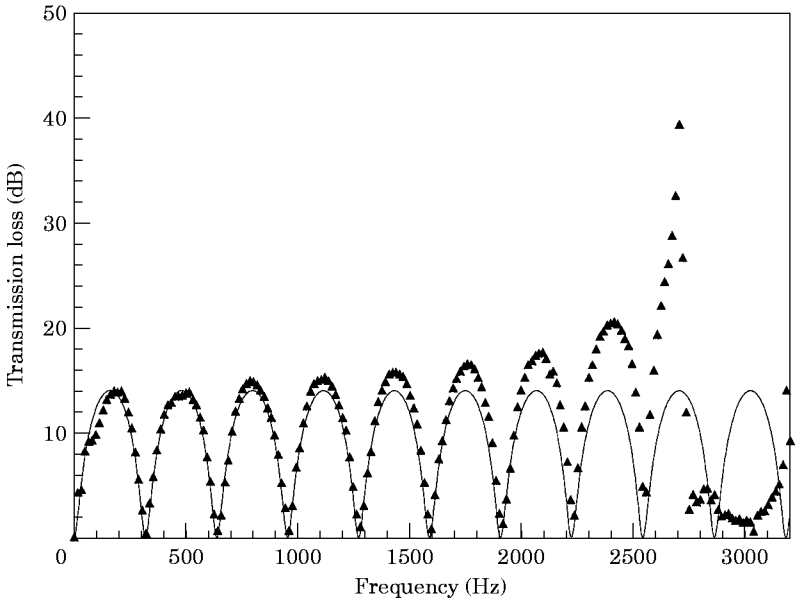

Figure 3. A transmission loss comparison between one-dimensional theory and experiment for an expansion chamber with $l/d = 3{\cdot}525$: ——, one-dimensional theory; ▲, experimental.

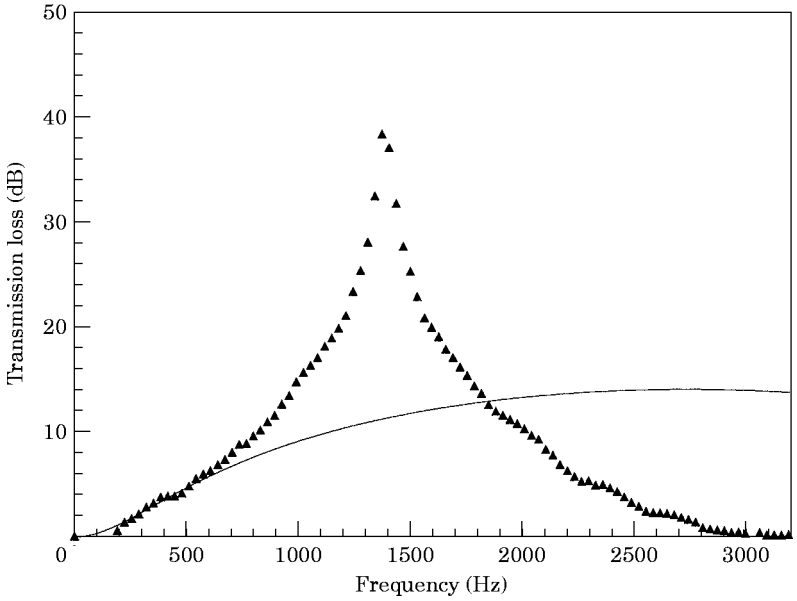

Figure 4. A transmission loss comparison between one-dimensional theory and experiment for an expansion chamber with $l/d = 0{\cdot}205$: ——, one-dimensional theory; ▲, experimental.

$$(U_{zC} + U_{zD})|_{z=l} = 0, \qquad r_1 \leqslant r \leqslant r_2. \tag{16}$$

Using the same procedure as for the expansion, equation (14) gives, for $s = 0$,

$$C_0\left(\frac{r_1^2}{2}\right)\mathrm{e}^{-\mathrm{j}kl} + \sum_{n=1}^{\infty} C_n\left[\frac{r_1 \mathrm{J}_1(\gamma_{2,0n} r_1)}{\gamma_{2,0n}}\right]\mathrm{e}^{\mathrm{j}k_{2,0n}l} + D_0\left(\frac{r_1^2}{2}\right)\mathrm{e}^{\mathrm{j}kl}$$

$$+ \sum_{n=1}^{\infty} D_n\left[\frac{r_1 \mathrm{J}_1(\gamma_{2,0n} r_1)}{\gamma_{2,0n}}\right]\mathrm{e}^{-\mathrm{j}k_{2,0n}l} - E_0\left(\frac{r_1^2}{2}\right) = 0 \tag{17}$$

and, for $s = 1, 2, \ldots, \infty$,

$$\sum_{n=1}^{\infty} C_n\left[\frac{\gamma_{2,0n} r_1 \mathrm{J}_1(\gamma_{2,0n} r_1)\mathrm{J}_0(\gamma_{1,0s} r_1)}{\gamma_{2,0n}^2 - \gamma_{1,0s}^2}\right]\mathrm{e}^{\mathrm{j}k_{2,0n}l}$$

$$+ \sum_{n=1}^{\infty} D_n\left[\frac{\gamma_{2,0n} r_1 \mathrm{J}_1(\gamma_{2,0n} r_1)\mathrm{J}_0(\gamma_{1,0s} r_1)}{\gamma_{2,0n}^2 - \gamma_{1,0s}^2}\right]\mathrm{e}^{-\mathrm{j}k_{2,0n}l} - E_s\left[\frac{r_1^2}{2}\mathrm{J}_0^2(\gamma_{1,0s} r_1)\right] = 0. \tag{18}$$

From equations (15) and (16) for $s = 0$,

$$C_0 r_2^2\,\mathrm{e}^{-\mathrm{j}kl} - D_0 r_2^2\,\mathrm{e}^{\mathrm{j}kl} - E_0 r_1^2 = 0 \tag{19}$$

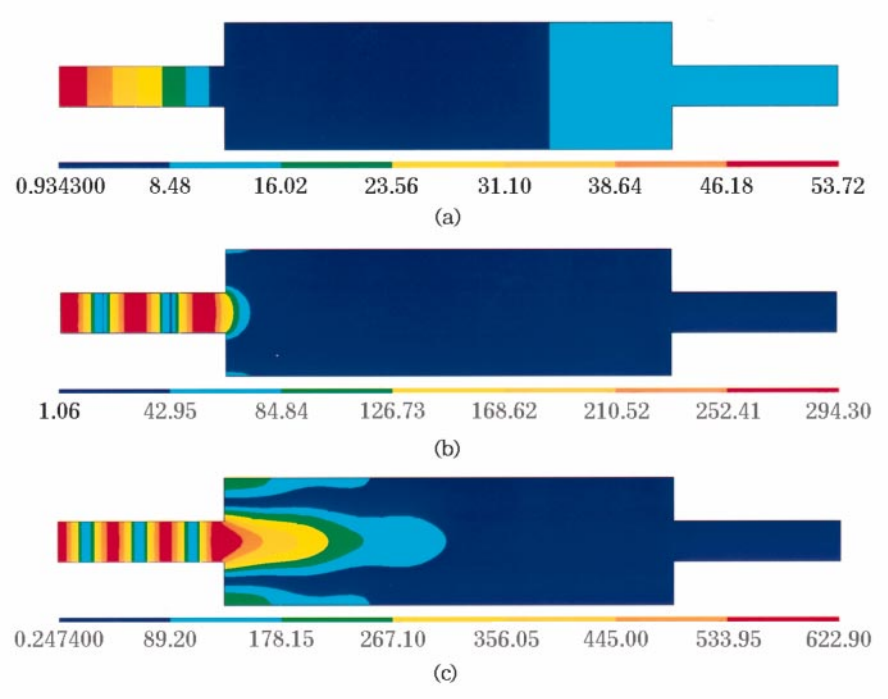

Figure 5. Pressure contours for an expansion chamber with $l/d = 3{\cdot}525$ for three frequencies of maximum transmission loss: (a) 160 Hz; (b) 2080 Hz; (c) 2714 Hz.

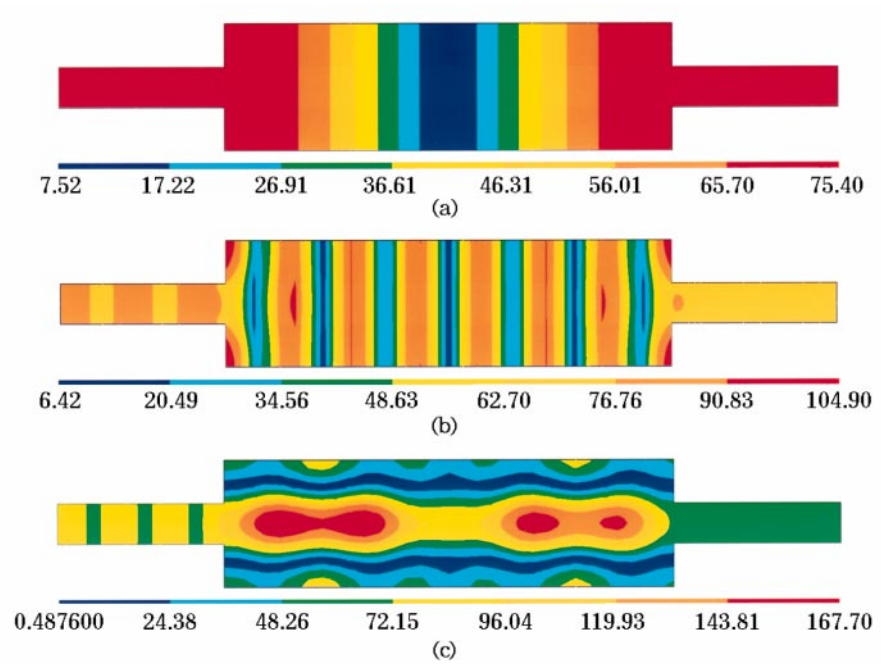

Figure 6. Pressure contours for an expansion chamber with $l/d = 3{\cdot}525$ for three frequencies of minimum transmission loss: (a) 320 Hz; (b) 2240 Hz; (c) 2800 Hz.

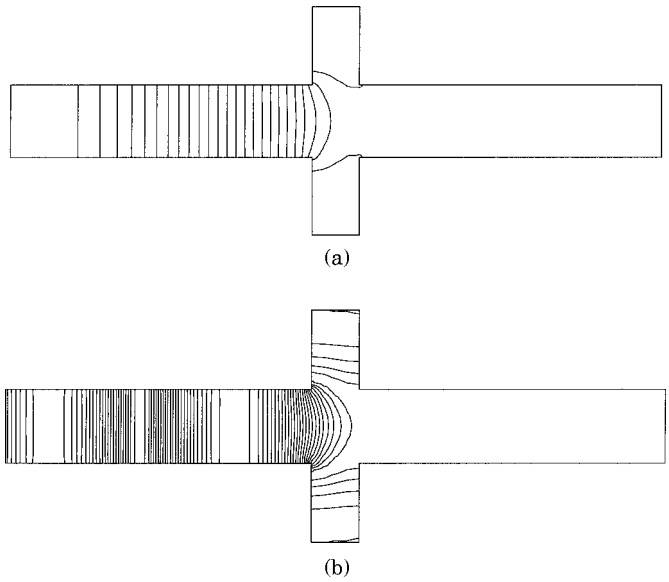

Figure 7. Lines of constant pressure for an expansion chamber with $l/d = 0{\cdot}205$ before and at resonance: (a) 160 Hz; (b) 1420 Hz.

and, for $s = 1, 2, \ldots, \infty$,

$$k_{2,0s}C_s\left[\frac{r_2^2}{2}\,\mathrm{J}_0^2(\gamma_{2,0s}r_2)\right]\mathrm{e}^{\mathrm{j}k_{2,0s}l} - k_{2,0s}D_s\left[\frac{r_2^2}{2}\,\mathrm{J}_0^2(\gamma_{2,0s}r_2)\right]\mathrm{e}^{-\mathrm{j}k_{2,0s}l} + kE_0\left[\frac{r_1\mathrm{J}_1(\gamma_{2,0s}r_1)}{\gamma_{2,0s}}\right]$$

$$-\sum_{n=1}^{\infty} E_n k_{1,0n}\left[\frac{\gamma_{2,0s}r_1\mathrm{J}_1(\gamma_{2,0s}r_1)\mathrm{J}_0(\gamma_{1,0n}r_1)}{\gamma_{2,0s}^2 - \gamma_{1,0n}^2}\right] = 0. \tag{20}$$

Equations (10)–(13) and (17)–(20) give a large (theoretically infinite) number of relations $(4s + 4)$ for a large number of unknowns $(4n + 4)$. The unknowns are the pressure coefficients for the incident and reflected waves in the inlet pipe, the chamber, and the outlet pipe (B_n, C_n, D_n and E_n, where $n = 0, 1, \ldots, \infty$ is the number of radial modes).

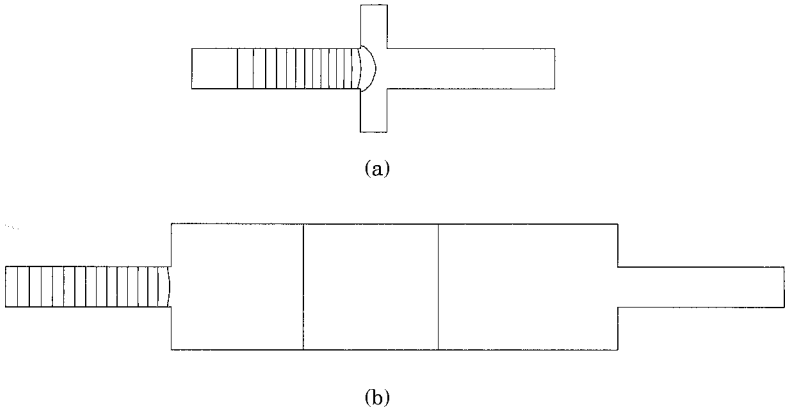

Figure 8. Lines of constant pressure for expansion chambers with (a) $l/d = 0{\cdot}205$ and (b) $l/d = 3{\cdot}525$ at 160 Hz (shown with equal contour strengths).

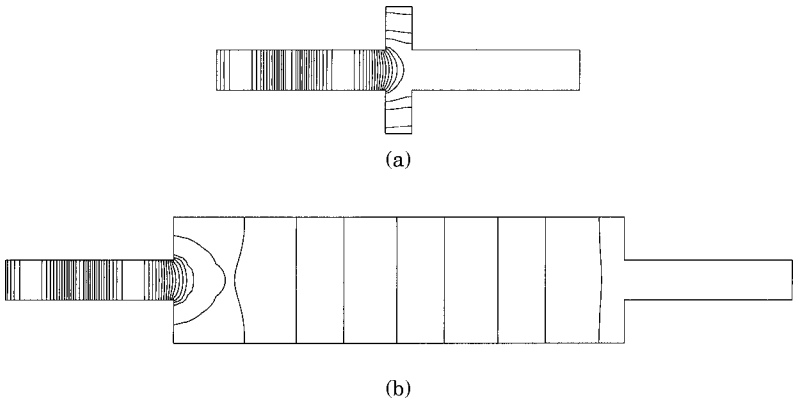

Figure 9. Lines of constant pressure for expansion chambers with (a) $l/d = 0{\cdot}205$ and (b) $l/d = 3{\cdot}525$ at 1420 Hz (shown with equal contour strengths).

Fortunately, higher modes have a diminishing effect on the solution, and s and n can be truncated to p terms resulting in $4p + 4$ equations with $4p + 4$ unknowns. The number of terms, p, needed for a converged solution depends both on the magnitude of the area transition and the length of the chamber. El-Sharkawy and Nayfeh [3] reported for their configurations that five terms were sufficient to converge to 0.1% accuracy. For the geometries and frequencies investigated here, five terms were found to be sufficient for the long chambers, but in excess of 15 terms were needed for very short chambers due to the high radial dependence. Once equations (10)–(13) and (17)–(20) are solved, the transmission loss is determined in the center of the tube by

$$TL = -20 \log_{10} \left| E_0 \, \mathrm{e}^{-\mathrm{j}kl'} + \sum_{n=1}^{p} E_n \, \mathrm{e}^{\mathrm{j}k_{1,0n}l'} \right| \tag{21}$$

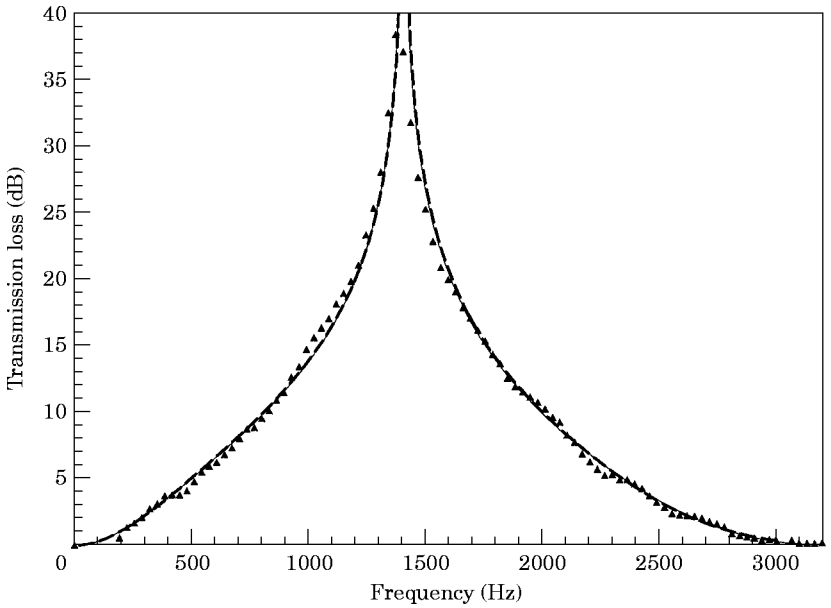

Figure 10. A transmission loss comparison between the 2-D analytical, the 3-D boundary element method and experimental results for an expansion chamber with $l/d = 0{\cdot}205$: ——, analytical; – –, 3-D boundary element; ▲, experimental.

(recall that the inlet pressure A is unity). Consider, for example, the extreme frequency of 3200 Hz used in the experiments. The first two values of $k_{1,0n}$ are $k_{1,01} = \mathrm{j}146{\cdot}5$ and $k_{1,02} = \mathrm{j}282{\cdot}8$, which produce exponentially decaying terms of $\mathrm{e}^{-146{\cdot}5l'}$ and $\mathrm{e}^{-282{\cdot}8l'}$ in the summation of equation (21). Thus, even for a short distance l', the non-planar modes leaving the expansion chamber decay and have a negligible effect on the transmission loss.

For the one-dimensional case, setting $p = 0$ in equations (10)–(13) and (17)–(20) gives four equations and four unknowns, which can be arranged to yield the classical transmission loss of a one-dimensional expansion chamber, as

$$TL = 10 \log_{10}\left[1 + \tfrac{1}{4}\left(m - \frac{1}{m}\right)^2 \sin^2 kl\right], \tag{22}$$

where $m = (d_2/d_1)^2$ is the expansion ratio (see, for example, Davis *et al*. [1]). Equation (22) reveals that the transmission loss for a one-dimensional expansion chamber oscillates between a minimum of zero when $kl = q\pi$ and a maximum when $kl = (2q - 1)\pi/2$, where $q = 1, 2, \ldots, \infty$.

3. BOUNDARY ELEMENT METHOD

In order to determine the multi-dimensional effects on the acoustic performance of expansion chambers, a three-dimensional direct boundary element method was used. This method is based on the Helmholtz equation:

$$\nabla^2 P^* + k^2 P^* = 0, \tag{23}$$

where $P = P^* \mathrm{e}^{\mathrm{i}\omega t}$. Given an enclosed smooth surface and two points X and Y, where Y is on the surface of the model, equation (23) can be written in an integral form as [9]

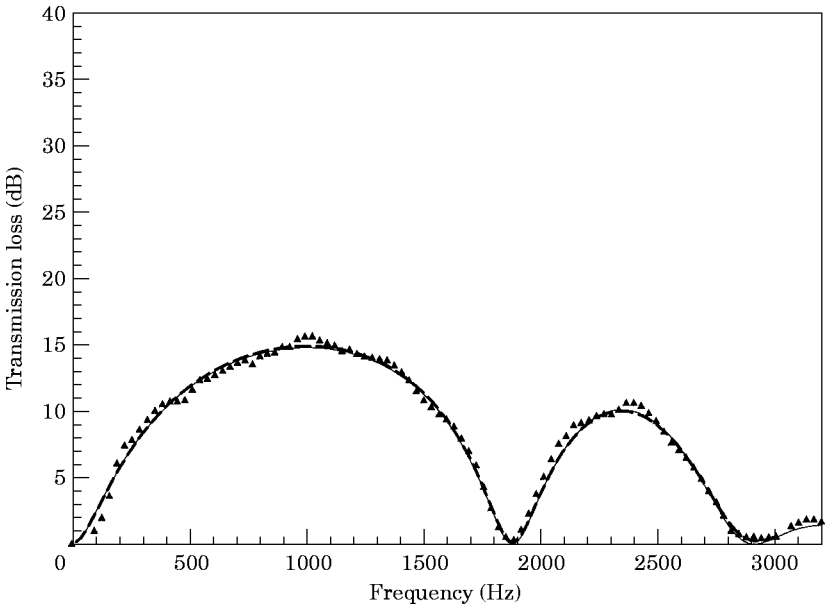

Figure 11. A transmission loss comparison between the 2-D analytical, the 3-D boundary element method and experimental results for an expansion chamber with $l/d = 0{\cdot}612$: ——, analytical; – –, 3-D boundary element; ▲, experimental.

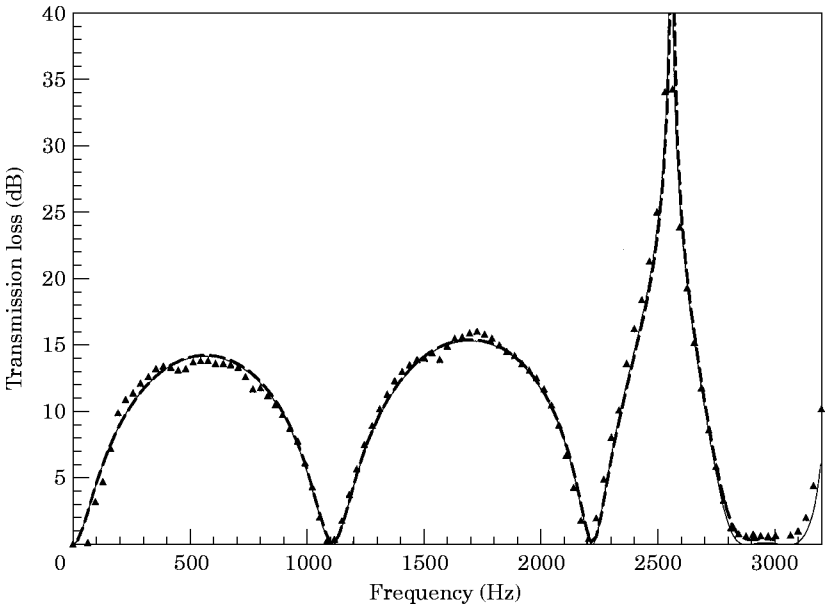

Figure 12. A transmission loss comparison between the 2-D analytical, the 3-D boundary element method and experimental results for an expansion chamber with $l/d = 1{\cdot}024$: ——, analytical; – –, 3-D boundary element; ▲, experimental.

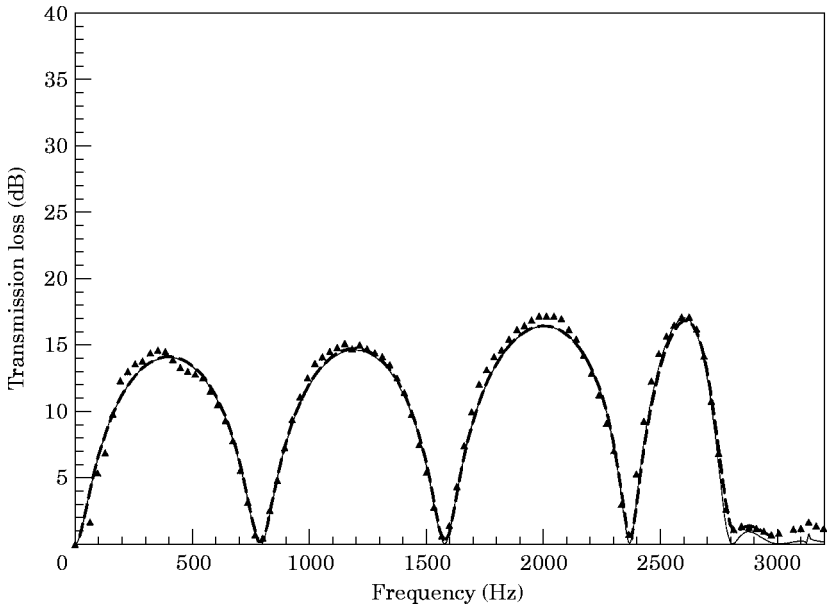

Figure 13. A transmission loss comparison between the 2-D analytical, the 3-D boundary element method and experimental results for an expansion chamber with $l/d = 1{\cdot}435$: ——, analytical; – –, 3-D boundary element; ▲, experimental.

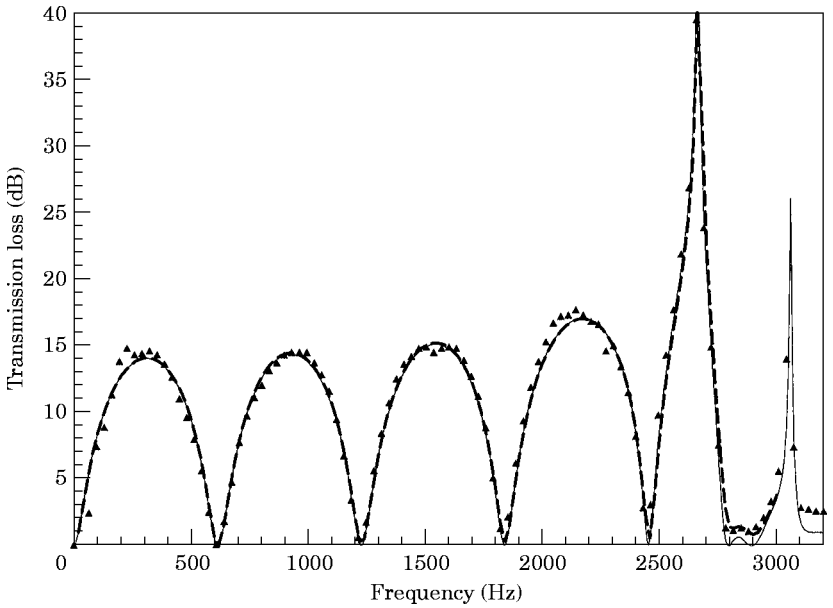

Figure 14. A transmission loss comparison between the 2-D analytical, the 3-D boundary element method and experimental results for an expansion chamber with $l/d = 1{\cdot}843$: ——, analytical; – –, 3-D boundary element; ▲, experimental.

$$\int_S \left[G(X, Y) \frac{\partial}{\partial n_Y} P^*(Y) - P^*(Y) \frac{\partial}{\partial n_Y} G(X, Y) \right] \mathrm{d}S_Y$$

$$= \begin{cases} \frac{1}{2}P^*(X), & \text{if } X \text{ is on a smooth surface,} \\ P^*(X), & \text{if } X \text{ is in the interior of the model.} \end{cases} \tag{24}$$

Here, $G(X, Y) = \mathrm{e}^{-\mathrm{j}kR}/4\pi R$ is Green's free space function and R is the distance between X and Y. By discretizing the surface into a number of elements, equation (24) may be rearranged as a system of equations

$$[A](P^*) = [B](\partial P^*/\partial n). \tag{25}$$

For each surface element, either P^* or $\partial P^*/\partial n$ is given in terms of one of the following boundary conditions:

$$P^* = \bar{P}, \qquad \text{for specified pressure,}$$

$$\partial P^*/\partial n = -\mathrm{j}\rho\omega V, \qquad \text{for specified velocity,}$$

$$\partial P^*/\partial n = -\mathrm{j}\rho\omega P^*/Z, \qquad \text{for specified impedance.}$$

Solution of equation (25) on the surface reveals the unknown (either P^* or $\partial P^*/\partial n$) for each surface element. Once the surface values are known, equation (25) can be solved for interior points through direct substitution. A more detailed account of this method can be found in Seybert and Soenarko [10], Soenarko and Seybert [11] and Ciskowski *et al.* [12].

For this study, parabolic quadrilateral and triangular elements were used to discretize the surface, and a nodal spacing to ensure greater than six nodes per wavelength was

maintained throughout the frequency range. For the boundary element method, transmission loss was computed by modeling the acoustic element in an extended impedance tube set-up similar to the experimental study. The system is driven by an oscillating piston with specified velocity and an anechoic termination is modelled by setting the impedance of the outlet equal to the characteristic impedance of the fluid, ρc.

4. EXPERIMENTAL APPROACH

The experimental set-up consists of an extended impedance tube configuration, as shown in Figure 2, where the expansion chambers are placed between a broad-frequency noise source and an anechoic termination. The two-microphone technique [13, 14] is utilized to separate incident and reflected waves for calculation of the transmission loss across the element, with one microphone pair placed before and another one after the expansion chamber. Although multi-dimensional waves are excited in the expansion chambers, the impedance tube diameter of 4·859 cm ensures planar propagation at the microphones, with a cut-off frequency of 4149 Hz for non-symmetric modes. For further details of the experimental set-up, refer to Selamet *et al*. [15, 16].

5. RESULTS AND DISCUSSION

To validate the analytical and computational models, an experimental study is conducted with nine expansion chambers constructed at different lengths as shown in Table 1. For these nine configurations, the chamber expansion ratio, m, is held constant while the length to diameter ratio, l/d_2, is varied from 0·205 to 3·525.

In Figures 3 and 4 are shown transmission loss comparisons of the one-dimensional theory of equation (22) with the experimental results for the two extreme cases with the largest and smallest l/d_2 ratios (hereafter the subscript 2 is dropped for convenience). For

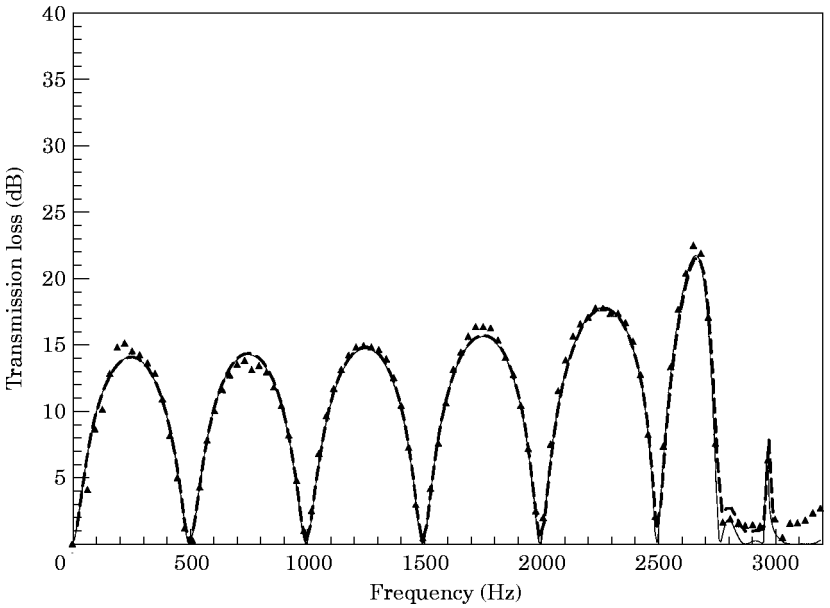

Figure 15. A transmission loss comparison between the 2-D analytical, the 3-D boundary element method and experimental results for an expansion chamber with $l/d = 2{\cdot}256$: ——, analytical; – –, 3-D boundary element; ▲, experimental.

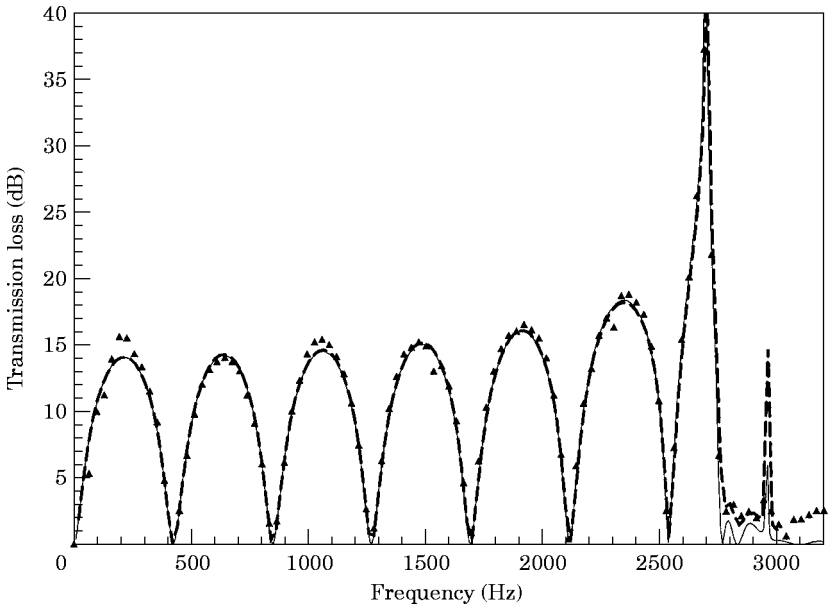

Figure 16. A transmission loss comparison between the 2-D analytical, the 3-D boundary element method and experimental results for an expansion chamber with $l/d = 2{\cdot}666$: ——, analytical; – –, 3-D boundary element; ▲, experimental.

the long expansion chamber, good agreement is shown in Figure 3 at low frequencies, whereas at higher frequencies noticeable magnitude differences are observed before the complete breakdown of the repeating one-dimensional domes. Based on acoustical theory, equation (3), the first radial (0, 1) cross-mode will propagate in the chamber at a frequency

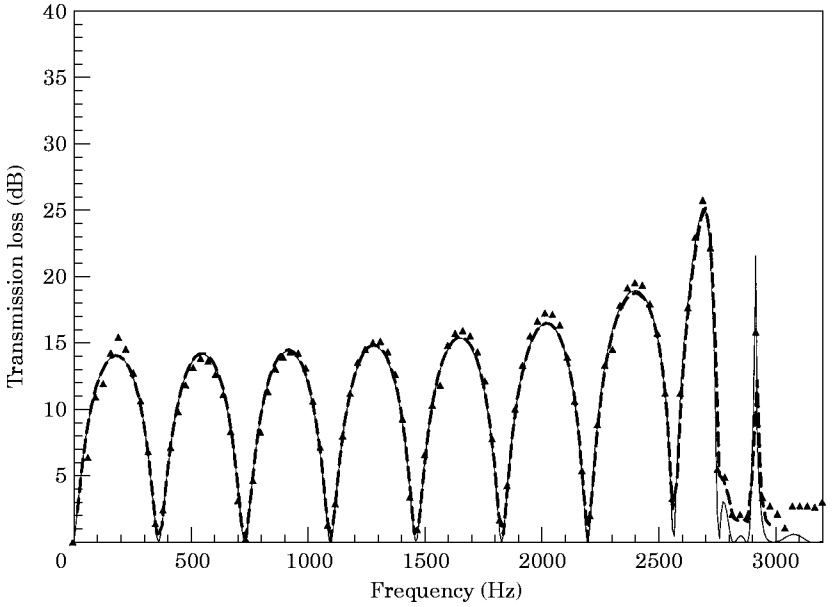

Figure 17. A transmission loss comparison between the 2-D analytical, the 3-D boundary element method and experimental results for an expansion chamber with $l/d = 3{\cdot}076$: ——, analytical; – –, 3-D boundary element; ▲, experimental.

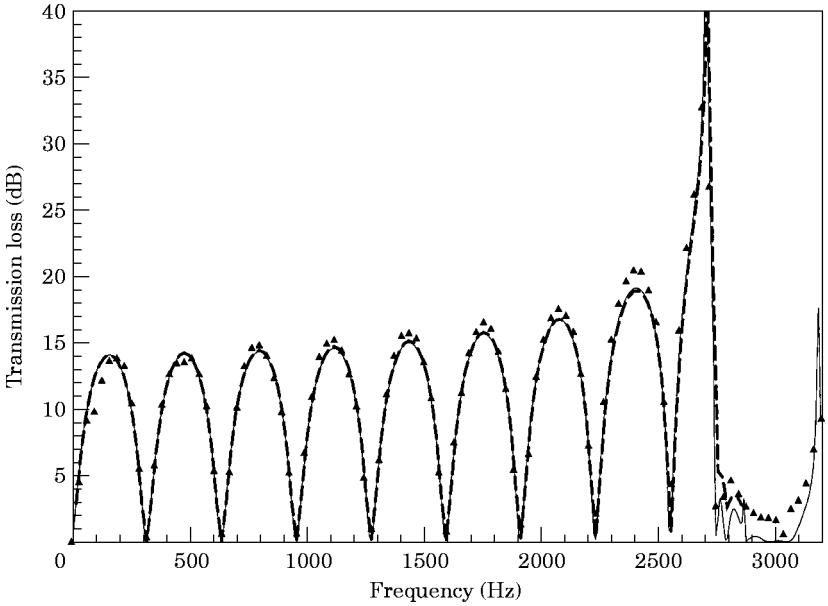

Figure 18. A transmission loss comparison between the 2-D analytical, the 3-D boundary element method and experimental results for an expansion chamber with $l/d = 3{\cdot}525$: ——, analytical; – –, 3-D boundary element; ▲, experimental.

of 2737 Hz. A final large transmission loss peak near this frequency at approximately 2714 Hz is shown in Figure 3. On the other hand, the short-length chamber of Figure 4 reveals (1) very little similarity between the one-dimensional prediction and the experimental results; and (2) peaks at a frequency well below the onset of any higher order modes.

The deviation of the experimental results from the one-dimensional analytical prediction suggests multi-dimensional wave propagation at frequencies at which, theoretically, only

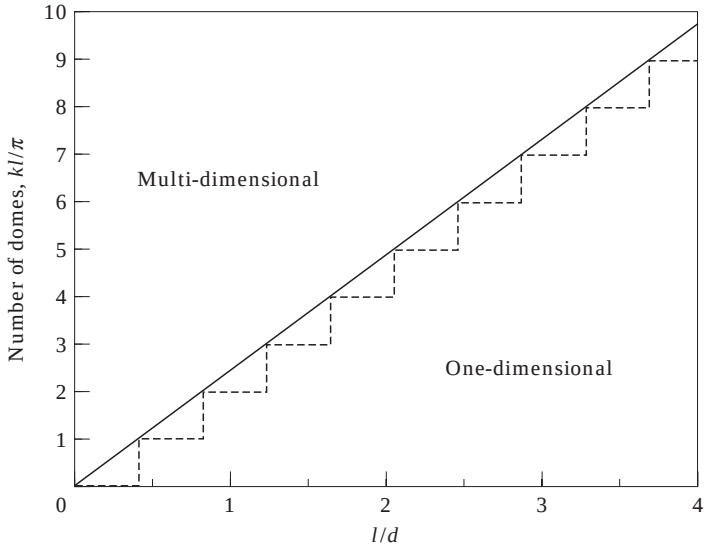

Figure 19. The predicted number of one-dimensional transmission loss domes versus the l/d ratio: ——, equation (28); – – –, equation (28) rounded to an integer number of domes.

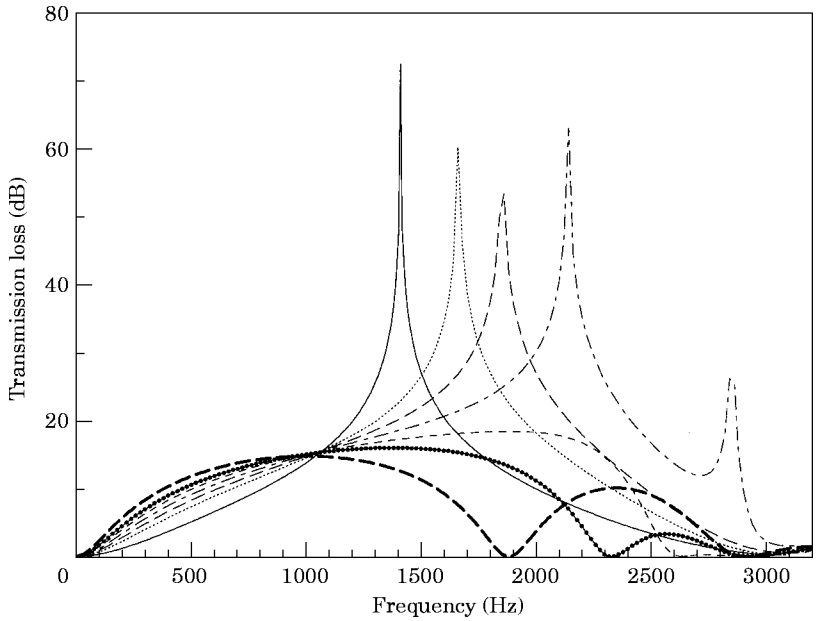

Figure 20. Two-dimensional analytical transmission loss predictions for expansion chambers with low length to diameter ratios: ——, l/d=0·205; ····, l/d = 0·3; — —, l/d = 0·35; —·—, l/d = 0·4; - - - -, l/d = 0·45; ●——●, l/d = 0·5; – –, l/d = 0·612.

the planar mode should propagate. In the available literature the multi-dimensional waves have been treated successfully by both finite element and boundary element methods. Some relevant applications of the former have been illustrated by, for example, Young and Crocker ([17] for a simple expansion chamber; [18] for exhaust mufflers including flow-reversing chambers and Helmholtz resonators), and by Sahasrabudhe *et al*. [19] for sudden area discontinuities. The present study employs the latter technique, as discussed in section 3. In terms of this three-dimensional boundary element method, the pressure fields inside the two extreme expansion chambers have been determined for several frequencies. In Figures 5 and 6 are shown the internal pressure contours for the $l/d = 3{\cdot}525$ chamber at three frequencies of maximum transmission loss and three frequencies of minimum transmission loss. These figures illustrate that at very low frequencies (Figures 5(a) and 6(a)), the contours are planar throughout the chamber, as expected. With increasing frequency, however, some non-planar contours begin to appear at the area discontinuities, due to the fact that the transition excites higher order radial modes. When the frequency is below that for which these modes can propagate freely (Figures 5(b) and 6(b)), the non-planar modes decay exponentially with distance and only planar behavior is observed away from the area transitions. As the frequency becomes closer to the propagating or cut-off frequency for the first radial (0, 1) mode in Figure 5(c), however, the modes do not decay as quickly and the multi-dimensional effects spread throughout the length of the chamber. Finally, Figure 6(c) shows a complete multi-dimensional behavior as the cut-off frequency for the first radial mode is exceeded.

Contours for the short $l/d = 0{\cdot}205$ chamber, shown in Figure 7, illustrate the importance of the multi-dimensional propagation even at low frequencies. Higher order modes are excited at the expansion and, due to the short length of the chamber, they do not decay sufficiently. In effect, this causes a "radial mode" to propagate in the chamber even through the frequency is almost half that of the cut-off frequency. A comparison between the two geometries with equal contour strength in Figure 8 at low frequency and in

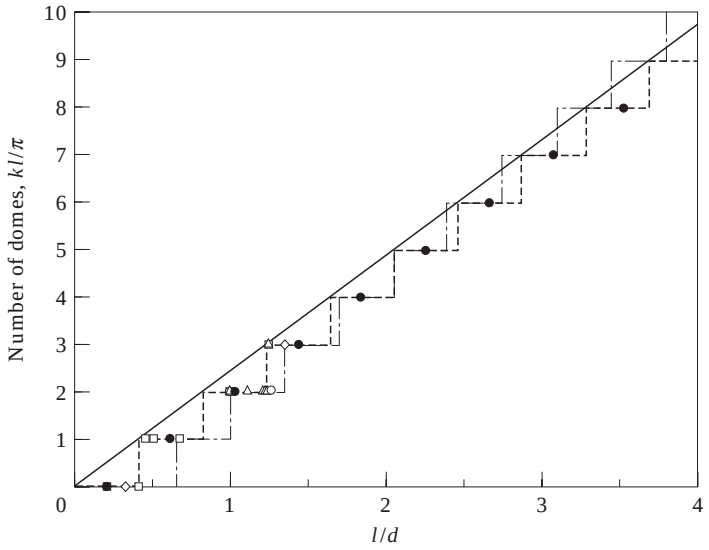

Figure 21. The predicted number of one-dimensional transmission loss domes versus the l/d ratio (a comparison with experiments and other works): ——, equation (28); — —, equation (28) rounded to an integer number of domes; –·–, equation (26); ●, experimental results (present study); □, Sahasrabudhe *et al*. (FEM); △, El-Sharkawy and Nayfeh (analytical); ◇, Ih and Lee (experimental, analytical); ○, Craggs (FEM).

Figure 9 at a higher frequency shows why the non-planar behavior is more significant in the shorter chamber.

The discrepancy between the one-dimensional results and the experiments, along with the multi-dimensional propagation at low frequency in the $l/d = 0{\cdot}205$ configuration, indicates that the diameter of the expansion chamber is not the only parameter affecting

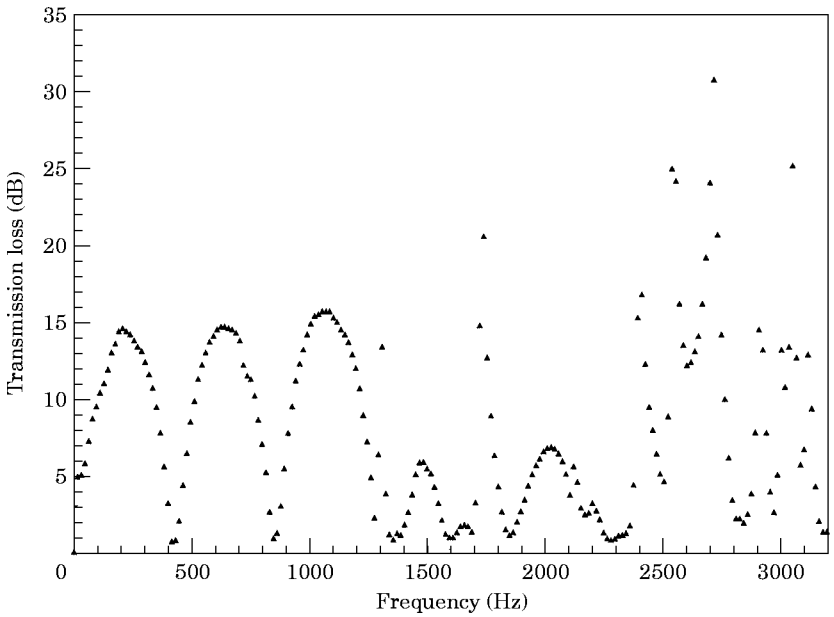

Figure 22. Experimental transmission loss results for an asymmetric expansion chamber with $l/d = 2{\cdot}666$, inlet and outlet offsets of 5·1 cm and rotated through 180 degrees; ▲, experimental.

the propagation of these non-planar waves and the length of the chamber needs to be taken into account. To study the length effect, nine expansion chambers listed in Table 1 were fabricated: the diameter of the chamber was held constant, while the length was varied. In Figures 10–18 are shown transmission loss comparisons among the experimental results, the two-dimensional analytical approach, and the three-dimensional boundary element method. As the l/d ratio of the chamber is decreased in Figures 10–18, the frequency range over which the repeating one-dimensional domes are observed decreases. This trend was also observed by Sahasrabudhe *et al*. [6] in a finite element study of different expansion chamber geometries. They developed an approximate relationship for the l/d ratio required to achieve plane wave behavior up to a frequency as

$$(l/d)_{q\pi} = 2(l/d)_{(q-1)\pi} - (l/d)_{(q-2)\pi}, \tag{26}$$

where $q\pi$ denotes the frequency kl. The first two l/d ratios are given as $(l/d)_{\pi} = 0{\cdot}65$ and $(l/d)_{2\pi} = 1{\cdot}0$.

In Figures 10–18 the one-dimensional repeating dome behavior is shown to prevail below the onset of the first radial mode (2737 Hz), while no domes extend beyond that frequency. Rearranging equation (3) yields the number of repeating domes, kl/π, as

$$\frac{kl}{\pi} < \frac{2\alpha_{mn}}{\pi}\left(\frac{l}{d}\right), \tag{27}$$

or

$$\text{number of domes} < 2{\cdot}440(l/d) \tag{28}$$

for concentric chambers, which is a relation between the l/d ratio of the chamber and the number of attenuation domes before higher order modes begin to dominate, as shown in Figure 19. This equation predicts that geometries with an l/d ratio of less than 0·41 will have no complete dome. This matches the value given by Ih and Lee [5] for the transition between the acoustically short and long expansion chambers. Analytical transmission loss curves for a number of short and single-domed chambers in Figure 20 also support this value. The predictions obtained by plotting equation (28) and rounding down to a complete number of domes, as shown in Figure 21, match the experimental results, as well as the results obtained from other authors, whereas equation (26) offers a reasonable guidance at low l/d ratios, while deviating slightly at high l/d. Equation (28) also provides an easier form to work with.

For all nine configurations, there is also a distinct trend in the transmission loss after the breakdown of one-dimensional propagation. For the cases with an even number of domes, the transmission loss exhibits a sharp peak, whereas for an odd number there is a transmission loss dome with a frequency band less than kl/π.

Although the present study concentrates on symmetric chambers, it is appropriate here to provide a few remarks on the non-symmetric configurations. Eriksson *et al*. [4, 20, 21] demonstrate the effect of inlet and outlet orientations on the frequency range over which the repeating dome behavior is observed. For example, by offsetting the inlet and outlet ducts from the center and placing them 180 degrees apart, the repeating dome behavior is observed until the geometry excites the first diametral (1, 0) mode. Similarly, by centering the inlet and offsetting the outlet, the repeating dome behavior is extented until the second radial (0, 2) mode propagates. For these non-symmetric configurations, the number of domes determined by introducing α_{mn}, which corresponds to the first higher order mode excited, into equation (27) may be shown to agree well with the experimental results given by Eriksson and his coworkers. In Figure 22, for example, are depicted the experimental

results for a configuration with offset inlet and outlet such that the (1, 0) mode is excited first. The combination of equation (27) with $\alpha_{10} = 1{\cdot}841$ from Table A1 and the l/d ratio of 2·666 yields three repeating domes, which agrees with the experimental results. A more thorough investigation of these asymmetric configurations, as well as their design implications, will be undertaken in the future.

6. CONCLUDING REMARKS

This study has investigated analytically, computationally and experimentally the effect of chamber length on the non-planar wave propagation in concentric expansion chambers. Multi-dimensional waves are excited at all frequencies at the area discontinuities of the chamber, however, for frequencies well below the cut-off frequency of the chamber, the multi-dimensional waves decay in a short distance and have little effect on the transmission loss. At higher frequencies approaching that of the first radial mode, however, multi-dimensional effects begin to dominate, causing the repeating dome behavior of the expansion chambers to break down. As the concentric expansion chamber length becomes short with $l/d < 0{\cdot}41$, the repeating dome behavior breaks down altogether, as the length of the chamber is no longer sufficient for the higher order modes to decay. This resonance behavior of acoustically short concentric chambers substantially below the cut-off frequency may, however, be desirable—particularly when coupled with the repeating dome attenuation of long chambers—for practical designs, as indicated by Eriksson *et al*. [4]. It is the combination of the length effect with the cut-off frequency that dictates the number of repeating domes. By taking both of these effects into account, an expression is given to relate the number of repeating transmission loss domes to the l/d ratio of the chamber, which may be useful to determine approximately the applicability of the simple one-dimensional predictions.

REFERENCES

1. D. D. Davis, G. M. Stokes, D. Moore and G. L. Stevens 1954 *NACA TN* 1192. Theoretical and experimental investigations of mufflers with comments on engine exhaust muffler design.
2. A. Craggs 1976 *Journal of Sound and Vibration* **48**, 377–392. A finite element method for damped acoustic systems: an application to evaluate the performance of reactive mufflers.
3. A. I. El-Sharkawy and A. H. Nayfeh 1978 *Journal of the Acoustical Society of America* **63**, 667–674. Effect of an expansion chamber on the propagation of sound in circular ducts.
4. L. J. Eriksson, C. A. Anderson, R. H. Hoops and K. Jayaraman 1983 *Proceedings* 11*th ICA*, *Paris*, 329–332. Finite length effects on higher order mode propagation in silencers.
5. J. Ih and B. Lee 1985 *Journal of the Acoustical Society of America* **77**, 1377–1388. Analysis of higher-order mode effects in the circular expansion chamber with mean flow.
6. A. D. Sahasrabudhe, M. L. Munjal and S. A. Ramu 1992 *Noise Control Engineering Journal* **38**, 27–38. Design of expansion chamber mufflers incorporating 3-D effects.
7. J. Miles 1944 *Journal of the Acoustical Society of America* **16**, 14–19. The reflection of sound due to a change in cross-section of a circular tube.
8. A. Selamet and P. M. Radavich 1995 *SAE* 950544, *SAE International Congress and Exposition*, *Detroit*, *Michigan*. The effect of length on the acoustic attenuation performance of concentric expansion chambers: an analytical, computational, and experimental investigation.
9. J. W. S. Rayleigh 1945 *The Theory of Sound*, *Volume II*. New York: Dover.
10. A. F. Seybert and B. Soenarko 1985 *Journal of the Acoustical Society of America* **77**, 362–368. An advanced computational method for radiation and scattering of acoustic waves in three dimensions.
11. B. Soenarko and A. F. Seybert 1991 *Proceedings of the* 6*th International Pacific Conference on Automotive Engineering*, *Seoul*, *South Korea*. Recent developments of the boundary element method to noise control problems in automotive engineering.

12. R. D. Ciskowski and C. A. Brebbia 1991 *Boundary Element Method in Acoustics*. Boston: Computational Mechanics Publications.
13. J. Y. Chung and D. A. Blaser 1980 *Journal of the Acoustical Society of America* **68**, 907–913. Transfer function method of measuring in-duct acoustic properties: I, theory.
14. *ASTM E* 1050-90 1990 *American Society for Testing and Materials*, *Philadelphia*, *PA*. Standard test method for impedance and absorption of acoustical materials using a tube, two microphones and a digital frequency analysis system.
15. A. Selamet, N. S. Dickey and J. M. Novak 1994 *Journal of the Acoustical Society of America* **96**, 3177–3185. The Herschel–Quincke tube: a theoretical, computational, and experimental investigation.
16. A. Selamet, N. S. Dickey and P. M. Radavich 1994 *SAE* 940612. Theoretical, computational, and experimental investigation of Helmholtz resonators: one-dimensional versus multi-dimensional approach.
17. C. J. Young and M. J. Crocker 1975 *Journal of the Acoutical Society of America* **57**, 144–148. Prediction of transmission loss in mufflers by the finite-element method.
18. C. J. Young and M. J. Crocker 1977 *Noise Control Engineering* **9**, 86–93. Finite element acoustical analysis of complex muffler systems with and without wall vibrations.
19. A. D. Sahasrabudhe, M. L. Munjal and S. Anantha Ramu 1995 *Journal of Sound and Vibration* **185**, 515–529. Analysis of inertance due to the higher order mode effects in a sudden area discontinuity.
20. L. J. Eriksson 1980 *Journal of the Acoustical Society of America* **68**, 545–550. Higher order mode effects in circular ducts and expansion chambers.
21. L. J. Eriksson 1981 *Noise-Con* '81, 105–110. Design implications of higher order mode propagation in silencers.
22. L. E. Kinsler, A. R. Frey, A. B. Coppens and J. V. Sanders 1982 *Fundamentals of Acoustics*. New York: John Wiley.
23. M. L. Munjal 1987 *Acoustics of Ducts and Mufflers*. New York: John Wiley.

APPENDIX A: THE PRESSURE FIELD

The linearized wave equation for the propagation of acoustical waves is

$$\nabla^2 P = \frac{1}{c^2}\frac{\partial^2 P}{\partial t^2}, \tag{A1}$$

where c is the speed of sound in the fluid [22]. For waves travelling in a circular pipe of radius r_i, the solution to equation (A1) is given, in cylindrical co-ordinates [7, 23], by

$$P(r, \theta, z, t) = \sum_{m=0}^{\infty}\sum_{n=0}^{\infty} A_{mn} \mathrm{J}_m(\gamma_{i,mn} r)\, \mathrm{e}^{\mathrm{j}(\omega t \pm k_{i,mn} z + m\theta)}, \tag{A2}$$

where m and n designate the diametral and radial mode numbers, A_{mn} is the pressure coefficient for each mode, ω is the angular frequency, J_m is the Bessel function of the first kind of order m,

$$k_{i,mn}^2 = k^2 - \gamma_{i,mn}^2, \tag{A3}$$

TABLE A1

The roots, α_{mn}, of the Bessel function $\mathrm{J}'_m(\alpha_{mn}) = 0$

m	$n = 0$	$n = 1$	$n = 2$	$n = 3$	$n = 4$
0	0	3·832	7·016	10·174	13·324
1	1·841	5·331	8·536	11·706	14·864
2	3·054	6·706	9·970	13·170	16·348
3	4·201	8·015	11·346	14·586	17·789
4	5·318	9·282	12·682	15·964	19·196

in which $k = \omega/c$ is the planar wavenumber, and, from the radial boundary condition at $r = r_i$,

$$\gamma_{i,mn} = \alpha_{mn}/r_i, \tag{A4}$$

where α_{mn} are the roots of the Bessel function $J'_m(\alpha_{mn}) = 0$. The first few values of α_{mn} are given in Table A1.

For pipes with circular cross-section, the diametral modes are not excited (assuming axially symmetric excitation) and can be neglected by setting $m = 0$ in equation (A2). Furthermore, separating out the planar mode from the radial ones yields the pressure field in the pipe as

$$P = A_0 \, e^{j(\omega t \pm kz)} + \sum_{n=1}^{\infty} A_n J_0(\gamma_{i,0n} r) \, e^{j(\omega t \pm k_{i,0n} z)}. \tag{A5}$$

APPENDIX B: NOMENCLATURE

A, B, C, D, E, F	pressure coefficients
c	speed of sound
d	diameter
f	frequency
G	$= e^{-jkR}/4\pi R$, Green's function
j	$= \sqrt{-1}$, imaginary unit
J_m	Bessel function of the first kind
k	planar wavenumber
$k_{i,mn}$	axial wavenumber
l	expansion chamber length; downstream microphone location
m	diametral mode number; expansion ratio
n	radial mode number; unit outward normal
p	truncation terms from infinite summations
P, P^*	acoustic pressure
q	$= kl/\pi$, number of domes
r	cylindrical co-ordinate; radius
R	distance between X and Y
s	orthogonal expansion terms
S	surface
t	time
TL	transmission loss
U	acoustic velocity
V	surface velocity
X	interior or surface point
Y	surface point
z	cylindrical co-ordinate
Z	$= P/V$, surface impedance
α_{mn}	zeros of $J'_m(\alpha_{mn}) = 0$
$\gamma_{i,mn}$	radial wavenumber
θ	cylindrical co-ordinate
ρ	density
ω	$= 2\pi f$, angular frequency